Journal of Molecular Graphics and Modelling 123 (2023) 108501

Contents lists available at ScienceDirect

Journal of Molecular Graphics and Modelling

journal homepage: www.elsevier.com/locate/jmgm

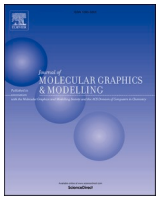

Molecular dynamics simulation of ssDNA and cationic polythiophene

Nehir Nalıncı Barbak, Erman Kıbrıs, Fethi Can Demirci, Nuran Elmacı Irmak *

Faculty of Science, Department of Chemistry, Izmir Institute of Technology, 35430, Urla, Izmir, Turkiye

A R T I C L E I N F O

Keywords:
Polyelectrolyte
Cationic polythiophene
ssDNA
Molecular dynamics simulation
NAMD
MM-PBSA

A B S T R A C T

In this work, molecular dynamics simulations of complexes composed of single strand DNA (ssDNA) sequences and cationic oligothiophenes are performed to understand experimental findings and the sensing ability of polythiophene electrolytes toward ssDNA. The simulation results exhibit no significant structural effect for replacing the cationic amine moiety with imidazole derivative on the side group of the oligomer. Adding a homopurine strand elongates the oligomer backbone; on the contrary, mixing up the homopyrimidine strand causes compression. On the other hand, these ssDNAs do not notably affect the compactness of the oligomer backbones. The anion-cation interactions play an essential role in the structural and spectroscopic change of cationic polythiophenes (CPTs) upon complexation with ssDNAs. The red shift of CPTs in the UV-VIS spectra with the addition of homopurine strands might be explained by the strong anion-cation, weak π −cation interactions, and high binding affinities. Nonpolar interactions (vdW and SA) and complex solvation energies dominate binding free energies. Hydrogen interaction analyses show that oligomers most likely approach the ssDNAs from their backbone upon complexation except for the duplex containing homopyrimidine strand and oligothiophene possessing imidazole derivative side chain.

1. Introduction

Polyelectrolytes (PEs) are common semi-conductive polymers with hydrophilic ionic or ionizable side groups and hydrophobic π-conjugated backbone. The conjugated PEs have adjustable structural properties, so they have been widely synthesized and used in diverse areas such as targeted molecule detections, detecting genetic disorders, biomedical applications, solar cells, light-emitting diodes, and photovoltaics studies [1–3]. Moreover, they have an important place in the literature owing to their water solubility and sensitive optical responses to external factors (temperature, light, pH, solvent, binding to other molecules, etc.) [3,4].

Polythiophene (PT) and its derivatives are the most used water-soluble conjugated PEs. Their optical and electronic properties form a unique substructure for bio- and chemo-sensor developments. Because of their low toxicity and good photostability in living-cell experiments, they have been broadly studied for sensing biological targets such as polysaccharides, proteins, folic acid, adenosine triphosphate (ATP), deoxyribonucleic acid (DNA) [5–10]. In particular, cationic PTs (CPT) have a significant role in biosensor development to be selective and sensitive probes due to their intermolecular interaction with DNA. In 2005, Leclerc et al. [6] have been reported conformational transitions caused by the complexation of single-stranded DNA (ssDNA) with a CPT derivative. The optical signals were followed without labeling the target or probe to provide the specific detection of nucleic acids. The PTs with various cationic side groups have been synthesized and mixed with ssDNA at an equal molar ratio by Rubio-Magnieto and co-workers [2] to determine the effects of PTs' backbone structures and the behavior of charged groups when binding to DNA. Carreon et al. [4] have studied the suitability of CPTs, which contain tertiary and quaternary amine, to bind DNA by electrostatic interactions. Some studies about the electrostatic interactions between biological molecules like ssDNA or double-stranded DNA (dsDNA) and CPT derivative have been summarized by Zheng and He in 2014 [11]. The study shows that the fluorescence of the polymer is quenched when CPTs are mixed with ssDNA, and a color change has been observed from yellow to red. The formation of complexes has been tracked by UV–visible absorption spectroscopy, fluorescent spectroscopy, nuclear magnetic resonance (NMR), and circular dichroic (CD) spectroscopy. These results were accounted for by the structural changes from a random coil to a flat conformation upon complex formation [11]. Ammanath et al. [12] have recently developed a simple colorimetric and fluorescence probe by using PT derivative for profiling advanced glycation end products (AGEs).

The changes in the polymer structure and the interactions between

* Corresponding author.
E-mail address: nuranelmaci@iyte.edu.tr (N. Elmacı Irmak).

https://doi.org/10.1016/j.jmgm.2023.108501
Received 13 December 2022; Received in revised form 17 April 2023; Accepted 18 April 2023
Available online 2 May 2023

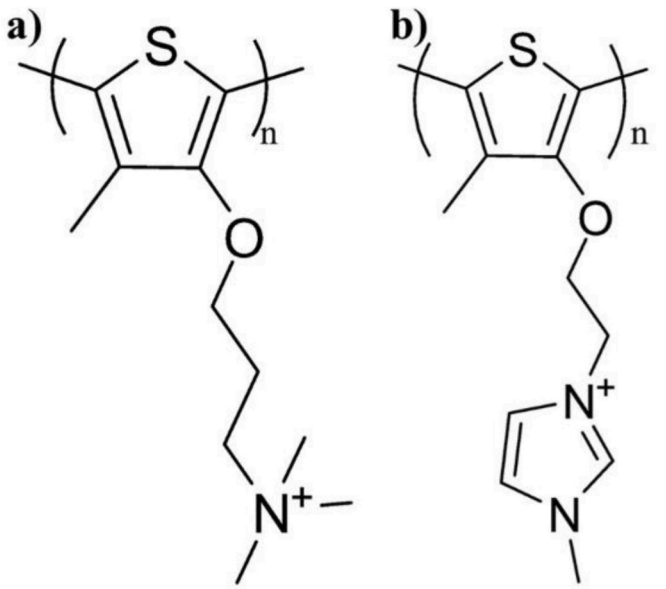

Fig. 1. The structure of a) poly- N, N, N-trimethyl-3-(4-methylthiophen-3-yl) oxy) propan-1-aminium, b) poly (1H-imidazolium-1-methyl-3-{2-[(4-methyl-3-thienyl)-oxy] ethyl}).

PT derivatives and DNA can be examined using computational methods. Molecular dynamics (MD) simulation is the most preferred computational method for large systems. One of the studies in the literature done by Preat et al. [13] in 2011 includes MD simulations of several duplexes formed by ssDNA and PT derivatives at the atomistic level. The possible interactions which triggered complex formation, such as electrostatic interactions (positive charges in PT derivatives and negative charges in DNA phosphates) and other specific interactions (O–H, S–H, π-π stacking, etc.), have been used in the analyses of their simulations. Another study in 2015 involved a combined experimental and computational work by Rubio Magnieto et al. [10]. Self-assembly between DNA and PT derivative has been linked to a balance between π-type and electrostatic intermolecular interactions. It has been indicated that MD simulation results support the experimental spectra (CD and UV–vis spectra). In our previous work [14], Chemistry at Harvard Macromolecular Mechanics (CHARMM) [15] compatible force field for a CPT derivative (see Fig. 1, a)) which has the potential of sensing biological molecules have been generated, and MD simulations for 20-mer and its complexes formed with AMP and ATP have been carried out. The response of the 20-mer to the addition of ATP causes a strong red shift in UV-VIS spectra. In that work, we have suggested that this might be explained by weak π-cation interactions in the ATP complex. These interactions may prevent the complex structure from a random coil form.

In the present work, CHARMM compatible force field has been generated for another CPT shown in Fig. 1b. MD simulations have been performed to investigate the nature of conformational changes in the CPT when ssDNA is added. The dominant type of interactions in the complexes will be explored via the MD simulation analyses to understand the behavior of complexes.

2. Materials and methods

The essential issue for performing MD simulations is the force field definition of the interested system. CHARMM-compatible force field parameters for poly- N, N, N-trimethyl-3-(4-methylthiophen-3-yl) oxy) propan-1-aminium (Oligomer 1; O1) have been generated by using force field Tool Kit (ffTK) [16]. The second CPT used in this study is poly (1H-imidazolium-1-methyl-3-{2-[(4-methyl-3-thienyl)-oxy] ethyl}) (Oligomer 2; O2), whose necessary potential constants are not present in the force field databases. These missed parameters have been generated in the content of this work by the same methods explained in the previous works [14,16–18]. The reported quantum calculation results have been obtained by the Gaussian09 program package [19]. The details are given in the supporting information (SI). The parameters for both ssDNA and water were taken from CHARMM libraries for nucleic acids (par_all36_na.prm), and TIP3P waters [20,21].

Table 1
The single-strand DNA sequences.

Name of strand	Sequence of strand
20A	5′- AAA AAA AAA AAA AAA AAA AA-3′
20T	5′- TTT TTT TTT TTT TTT TTT TT-3′

CPTs used in this work, O1, and O2, consist of 20 repeating units. ssDNAs modeled with 20 adenine (homopurine) and 20 thymine (homopyrimidine) nucleobases are shown in Table 1 and are named 20A and 20T, respectively. The initial structures for the complexes (O1-20A, O1-20T, O2-20A, O2-20T) have been created with Avogadro [22]. Initial and most probable (based on the average end-to-end distance value) configurations of O1, O2, and their complexes are given in Fig. 2.

All atomistic MD simulations were performed using Nanoscale Molecular Dynamics (NAMD) 2.12 package [23]. Visualizations of saved trajectories were obtained by Visual Molecular Dynamics (VMD) software [24]. The oligomers and their complexes with ssDNA were placed in the middle of the cubic simulation box with minimum possible dimensions, 90.0 × 90.0 × 90.0 Å, and water molecules (TIP3P model) were added to fill the box. The minimum distance between water and solute was taken as 2.4 Å (default value). Cl− ions were added to provide a charge balance for the oligomers in water. The counter ions were disregarded for their 20T and 20A complexes simulations because they were electrically neutral. The Particle-mesh Ewald (PME) algorithm was used for long-range electrostatics in all simulations. The cut-off was set to 14 Å. First, the system of interest was minimized by performing 20 ns simulations. Secondly, the systems were heated from 0 to 310 K gradually. After that, a 20 ns equilibration MD simulation at the NVT ensemble was done. Then a 100 ns production simulation at the NPT ensemble was performed with time step 2.0 fs. Three independent replicas of 100 ns production MD simulations were carried out. During the production steps, the coordinates and energy of systems were saved every 50 ps. The last 60 ns part of production simulations was used for the data analysis. The conformers at the average/most probable end-to-end distance (R_{ee}) values were selected for UV-VIS calculations.

The binding free energies between oligomers and ssDNA were estimated by Molecular Mechanics Poisson Boltzmann Surface Area (MM-PBSA) method [25], which has been widely used to predict binding affinity and energy decomposition. Calculation of Free Energy (CAFE) program [26] powered by NAMD and VMD was used to calculate free energies for oligomers, ssDNAs, and complexes.

3. Results and discussion

In this study, the complexation of O1 and O2 with ssDNAs has been investigated using MD simulations. The complexes were formed by pairing ssDNAs and the CPT derivatives. The oligomers of interest, O1, and O2, contain amine and imidazole moieties, respectively. The cationic side group effect of oligomer on complexation and sensor ability have been studied with these oligomers. Two different systems have been prepared using homopurine and homopyrimidine ssDNAs to examine the effects of the type of nucleobases on O1 and O2 complexes.

The absorption spectrum of CPTs with different cationic side groups has similar λmax values [6,7]. The UV-VIS spectra of the CPTs conducted in this work were used to validate the generated force field since there is no X-ray or NMR data in the literature (to our knowledge).

The UV-VIS spectra of CPTs in ssDNA complexes were calculated via Gaussian09 at the TD/HF/3-21G and TD/B3LYP/3-21G level of theory using the selected conformers of 20-mer. The computational and

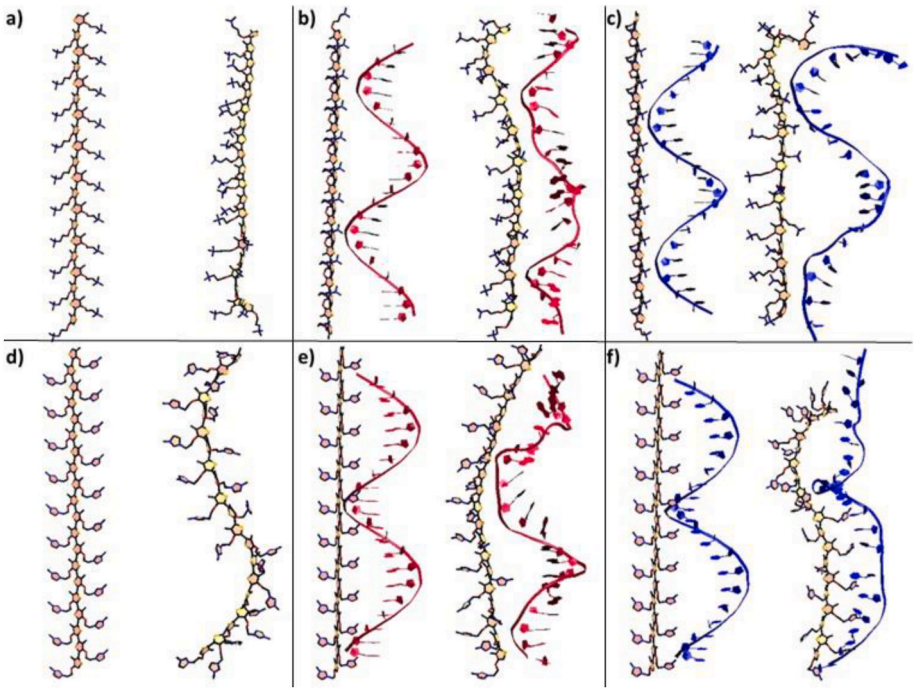

Fig. 2. The snapshots of initial (left) and average R_{ee} positions (right) of **a)** O1, **b)** O1-20A, **c)** O1-20T, **d)** O2, **e)** O2-20A, **f)** O2-20T.

Table 2
The computational UV-VIS absorption λmax values.

	λ(nm) B3LYP/3-21G	λ(nm) HF/3-21G		λ(nm) B3LYP/3-21G	λ(nm) HF/3-21G
O1	370[a]	290	**O2**	369[a]	282
O1-20A	377	306	**O2-20A**	380	294
O1-20T	374	297	**O2-20T**	373	283

(Li et al., 2006 for O1 (401 nm), Ho et al., 2005 for O2 (397 nm)).
[a] The experimental λ_{max}.

experimental (available in the literature) UV-VIS absorption *λmax* values are given in Table 2. The close experimental and computational (B3LYP/3-21G) UV-VIS absorption *λmax* values for O1 and O2 validate generated force field parameters.

There is a red shift in the UV–Vis spectrum of the cationic poly [3-(60-(trimethylphos-phonium) hexyl) thiophene-2,5-diyl] upon the addition of the ssDNAs (*λmax* ~ 520 nm) in the study of Rubio Magnieto et al. [10]. Based on their results, UV-VIS absorption measurements showed the longest red shift (nearly ~70 nm) for this CPT with a homopurine strand. Our results (**DFT** and HF) also demonstrate that O1-20A and O2-20A have a red shift (**7**/16 nm, and **11**/12 nm, respectively) in the UV–Vis spectrum. Similarly, O1-20T and O2-20T have a slight red shift by **4**/7 nm and **4**/1 nm, respectively (Note that bold-face numbers refer to DFT results). The experimental and theoretical results both showed a red shift in the presence of ssDNAs. Although they agreed on the trend of *λmax*, the quantities are not very similar. The reason for these differences can be related by two facts; i) the use of a low level of theory in the UV-VIS calculations due to the size of the systems and computational demands, and ii) stacking of complexes might be formed in experiments, whereas only one 20-mer of CPT with ssDNAs used in the simulations.

3.1. Molecular dynamics simulation results

$$\mathrm{RMSD} = \sqrt{\frac{1}{N}\sum_{i=1}^{N}\left(\vec{r}_{1,i} - \vec{r}_{0,i}\right)^2} \quad (1)$$

Time evolution of root mean squared deviations (RMSD) was calculated by using Eq. (1) (where N and $\vec{r}$ are numbers of atoms and the position vector of these atoms) to show that the simulations achieved the equilibration as demonstrated in Fig. 3. It should be noted that these RMSD values are for the production part of the simulations and the average values of three independent replicas. The conformations did not change much compared to the first configuration based on small RMSD values (the changes are lower than 5 Å). The structure of the oligomer backbone was analyzed over the last 60 ns part of simulations where the RMSD fluctuations are less than 1.5 Å, a sign of conformational stability. R_{ee} and radius of gyration (Rg) were calculated to measure how much the oligomer chain stretched out and compacted through the complexation.

The distance between two hydrogen atoms at first and the last thiophene ring of oligomers had been referred to as R_{ee}. The average R_{ee} values with error bars were displaced in Fig. 4. O1 and O2 have similar average R_{ee} values (67 and 66 Å). The oligomer backbones in adenine complexes have 1 and 3 Å longer end-to-end distances than oligomers in water, respectively. On the other hand, O1-20T (60 Å) has a smaller R_{ee} value than O1 and in its 20A complexes. At the same time, R_{ee} of the O2 backbone did not affect much by the presence of thymine ssDNA. This means that the oligomers elongated through complexation with the adenine strand. O1 is compressed with the thymine. O2 almost did not respond to the 20T addition.

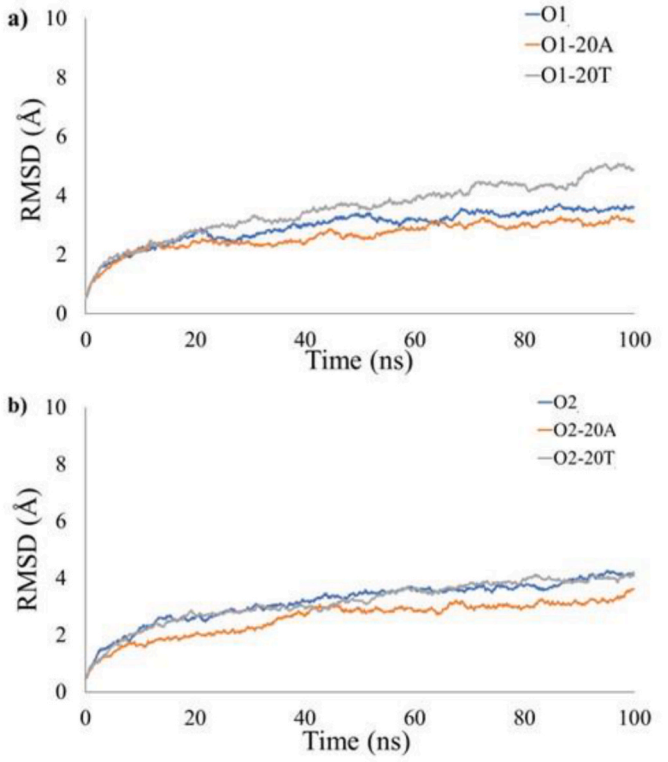

Fig. 3. Time evolution of RMSD of **a)** O1 (blue), O1-20A (orange), O1-20T (grey); **b)** O2 (blue), O2-20A (orange), O2-20T (grey). (For interpretation of the references to color in this figure legend, the reader is referred to the Web version of this article.)

$$\mathrm{Rg} = \sqrt{\frac{\sum_{a=1}^{N} m_a (r_a - r_{com})^2}{\sum_{a=1}^{N} m_a}} \tag{2}$$

The average Rg values, which demonstrate the compactness of the systems, were found from Eq. (2) and shown in Fig. 5. The mean Rg values were observed in the range of 21 Å and 22 Å. The oligomers' backbones in all conditions have similar compactness.

3.2. Interactions between CPTs and ssDNAs

Specific intermolecular interactions (like anion-cation, π-cation, and hydrogen) were examined to obtain the dominant interaction which causes the structural changes and spectroscopic behavior of oligomers under the influence of ssDNAs. These interactions were computed by measuring the distance between two atoms considered for analyses (see Fig. 6). The average number of all interactions was found by counting the distances less than the corresponding threshold value and dividing this value by the total frame number as 600. Then, these interactions were normalized by using their possible numbers.

The anion-cation interactions are measured by the distance from nitrogen atoms in the oligomer to oxygen atoms on the phosphates of ssDNA, and π -cation interactions are evaluated by the distance between the center of the six-membered ring of the nucleobases and the nitrogen atom of the oligomer. As mentioned in another study, the threshold distances were used to determine the number of interactions, and they were taken as 6.5 Å [13].

The number of anion-cation and π-cation interactions are shown in Fig. 7 for all oligomer complexes. The dominant interactions in all adenine complexes have electrostatic nature. O1-20T owns similar anion-cation and π -cation interactions, while O2-20T possesses

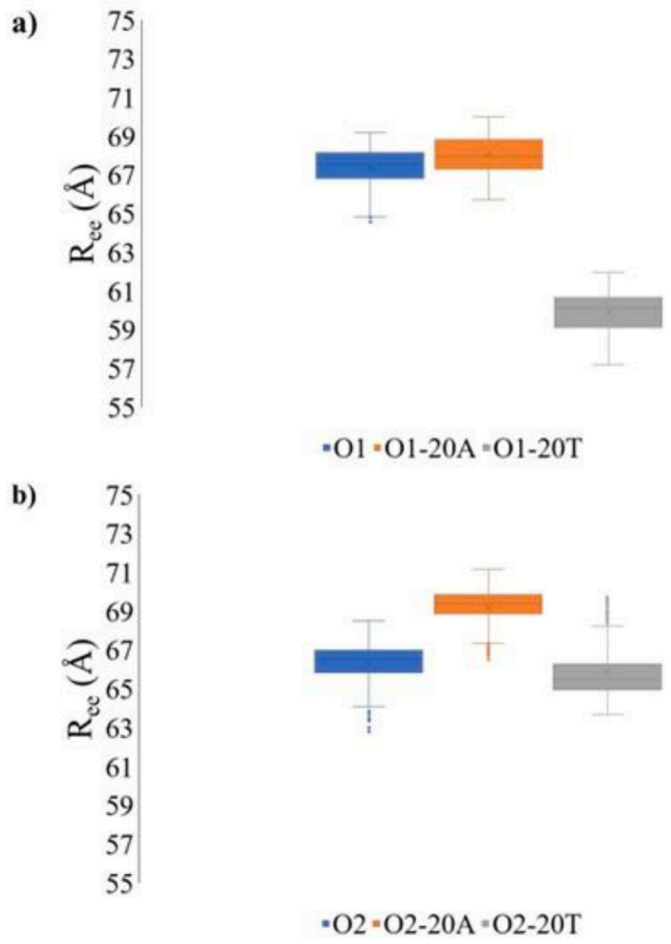

Fig. 4. R_{ee} values of **a)** O1 (blue), O1-20A (orange), O1-20T (grey); **b)** O2 (blue), O2-20A (orange), O2-20T (grey). (For interpretation of the references to color in this figure legend, the reader is referred to the Web version of this article.)

significant anion-cation interactions. O2 complexes almost lack π-cation interactions. Anion-cation interaction seems to play an important role in the structural and spectroscopic behavior of these complexes. The compression of the O1-backbone in the 20T complex might be explained by a strong π-cation and less anion-cation interactions. On the other hand, the weak π-cation interactions of O1 and O2 with 20A complexes could be related to the red shift of CPTs in the UV-VIS spectra with the addition of homopurine strands.

The number of hydrogen interactions for all complexes is shown in Fig. 8. Three types of hydrogen interactions were considered; O–H, H–O, and S–H. O–H refers to a number of cases in which the distance between oxygen atoms in oligomer and hydrogen atoms in ssDNA is shorter than 3 Å (threshold value). Similarly, H–O and S–H are used for the corresponding distances for the hydrogen atom of the oligomer – oxygen atoms of the ssDNA and sulfur atom of the oligomer – hydrogen atoms of the ssDNA, respectively (see Fig. 6). It should be noted that these are not assumed as hydrogen bonds since the angles are not considered.

Fig. 8 shows that almost no O–H interactions exist in all complexes, meaning oxygen atoms on oligomer are far from hydrogens on ssDNAs through the trajectories. On the other hand, S–H interactions are the dominant ones; sulfur atoms on the oligomer backbone like to be close to the hydrogen atoms on ssDNAs. All complexes have fewer HO interactions than SH, but in O2-20T, the difference is not remarkable.

To understand the role of side groups and the backbone of the oligomer in the structural change upon complexation with ssDNA, the fractions of these interactions coming from side parts and oligomer

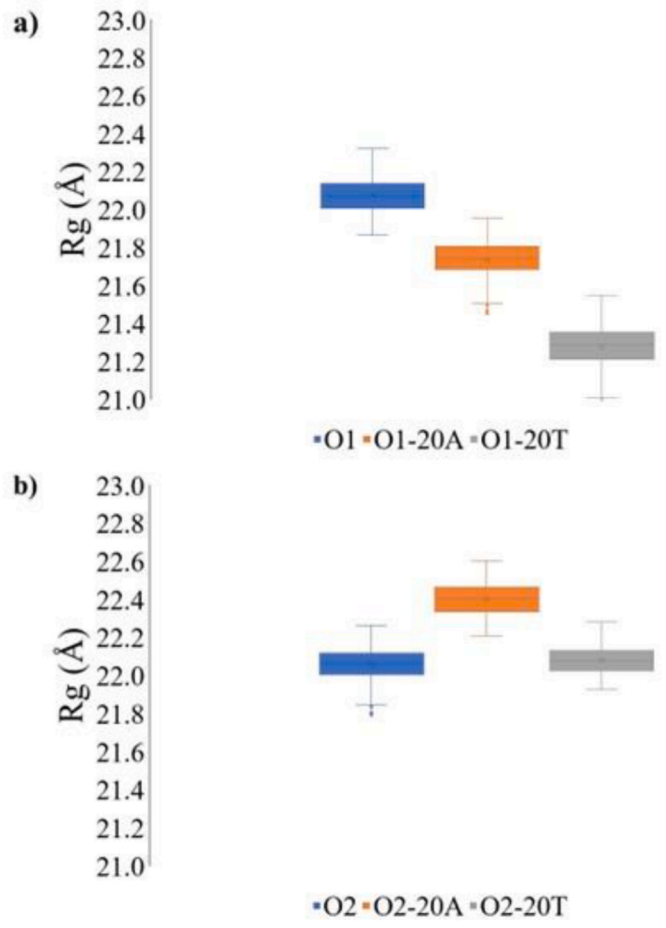

Fig. 5. Rg values of **a)** O1 (blue), O1-20A (orange), O1-20T (grey); **b)** O2 (blue), O2-20A (orange), O2-20T (grey). (For interpretation of the references to color in this figure legend, the reader is referred to the Web version of this article.)

skeleton are found by counting O–H, H–O (excluding hydrogens of methyl at oligomer backbone) for side-chain interactions and S–H interactions for the backbone (given in percentages). The percentages of interactions with the side groups and backbones are displayed in Fig. 9.

The contribution of the backbone interactions is much higher in the formation of the complexes. This means that the oligomers approach the ssDNAs from their backbone upon complexation. The side and backbone interactions play almost the same role in complexation for O2-20T since side interactions are only 20% lower than backbones.

3.3. Binding free-energy calculations (MM-PBSA) results

Binding affinities were predicted via the CAFE program based on the MM-PBSA method. The binding free energy is defined in Eq (3),

$$\Delta G_{bind} = G_{complex} - G_{oligomer} - G_{ssDNA} \tag{3}$$

$$\Delta G_{bind} = \Delta H - T\Delta S = \Delta E_{gas} + \Delta G_{sol}^{polar} + \Delta G_{sol}^{nonpolar} - T\Delta S \tag{4}$$

In MM-PBSA, the free energy consists of gas phase energy (E_{gas}), polar solvation free energy, and non-polar solvation energy. The entropy contribution ($T\Delta S$) to free energy is generally disregarded for structurally similar molecules because of high computational demands and the inaccuracy of methods used in entropy calculation.

The sum of the electrostatic energy (Elec) and the polar solvation (PB) energy; "polar energy," the sum of vdW interactions, and the non-

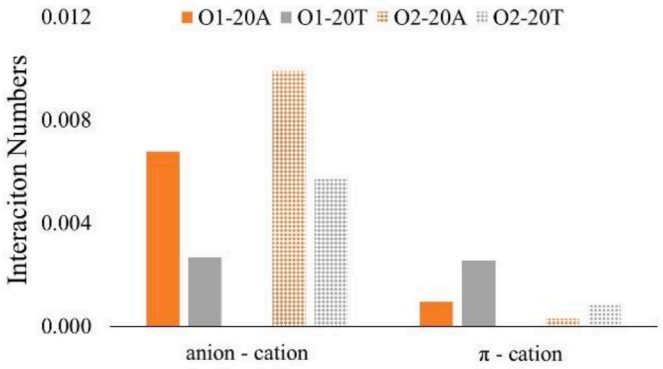

Fig. 7. Number of anion-cation and π-cation interactions between oligomers and ssDNAs along the simulations.

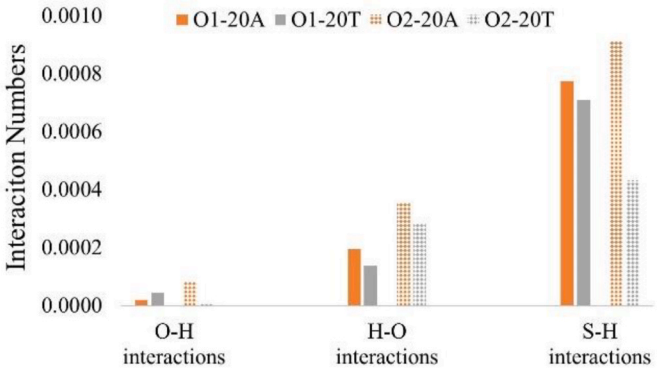

Fig. 8. Number of hydrogen interactions for all duplexes.

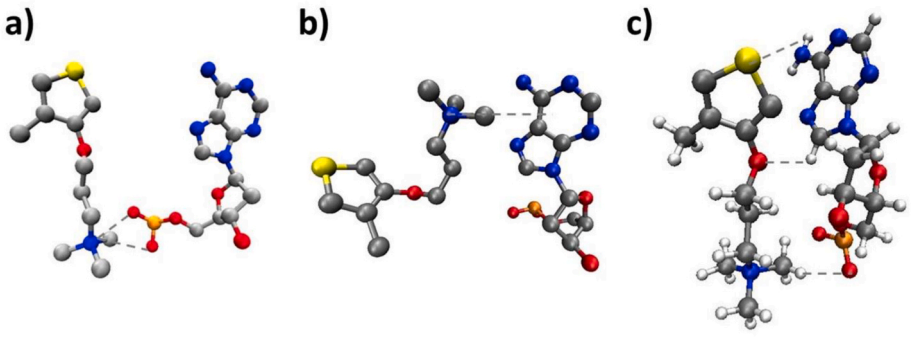

Fig. 6. The representation of **a)** the cation-anion, **b)** π - cation, and **c)** hydrogen interactions between oligomers and ssDNAs.

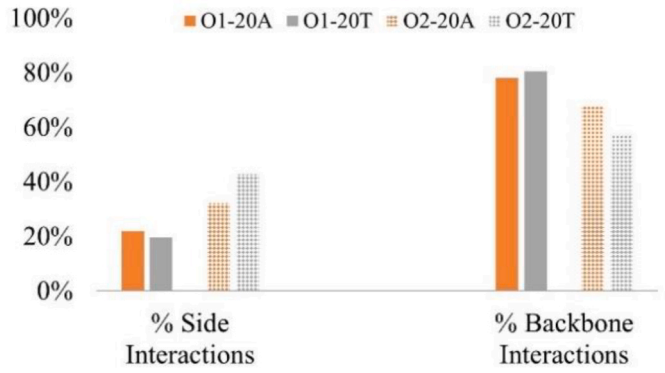

Fig. 9. The percentages of interactions of ssDNAs with the side groups and backbones of CPTs.

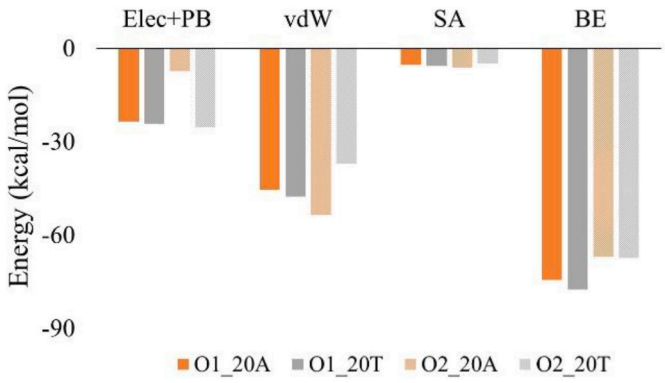

Fig. 10. Binding free energies and their decompositions of complexes (kcal/mol).

polar solvation (SA) energy: "nonpolar energy," binding free energy (BE) for the systems are shown in Fig. 10. Free energies of oligomers, ssDNAs, and their complexes and energy decomposition of them are given in SI (Fig. 6).

MM-PBSA calculations produce almost similar binding affinities to both ssDNAs for both oligomers. O1 complexes have about 10 kcal/mol lower binding energy values than O2 complexes. There is no dramatic binding energy difference between them.

Polar parts of energy constituents have almost the same magnitude but differ in signs (Table 3). Their absolute values are in the order of 5000 kcal/mol, and their sum is in the range of −7 kcal/mol and −25 kcal/mol. The vdW interactions and SA energy contribute nonpolar part of free energy, which falls [−42;-60] kcal/mol interval. These results reveal that the nonpolar interactions mostly dominate the binding affinity. Adenine complexes have smaller solvation energies than thymine complexes. The shortest complex (O1-20T) and the most extended complex (O2-20A) have the highest and lowest solvation energies, respectively. Elongation by 20A and compression by 20T of oligomers' backbones might be due to the solvation effect. The solvation affects the structure of the complexes. O1-20T has the most negative binding energy and the largest solvation energy. However, the opposite situation was observed in O2-20A. Complex solvation energy is another factor that plays a notable role in binding energies. O1 complexes have about 10 kcal/mol lower binding energy values than O2 complexes. Adenine complexes have longer end-to-end distances and higher binding free energies. O1-20T complex has the shortest R_{ee} value and highest binding affinity, meaning 20T binds more tightly than 20 A to the O1 oligomer.

4. Conclusions

In this work, we have carried out MD simulations of complexes formed by CPT derivatives and ssDNAs to understand the change in the UV-VIS spectra of CPT solutions by adding various ssDNAs. Two different cationic thiophene oligomers and ssDNA sequences were used to construct complexes. The effects of cationic side groups in PT electrolytes and the type of DNA sequences on the structure of the CPT backbone were studied. Rg, R_{ee} values have been used for the structural analysis to deduce how oligomers respond to ssDNAs. Binding affinities were estimated by using the MM-PBSA method. Hydrogen and electrostatic interactions were used to understand the experimental findings in UV-VIS spectra upon complexation.

It was observed that the compactness of the oligomer backbone was not affected much by the addition of ssDNAs. On the other hand, the extent of CPT backbones is influenced by ssDNAs, such that oligomers are compressed by adding thymine strand while they are stretched with the adenine complexation.

Anion-cation interactions play a significant role in the structural and spectroscopic change of CPTs through the mixing of ssDNAs. The anion-cation interactions are dominant in all adenine complexes. The cations of O2 mainly interact with the anions on ssDNAs for the thymine complex. However, O1-20T has almost the same anion and π-cation interactions. Based on these results, the red shift of CPTs in the UV-VIS spectra with the addition of homopurine strands is related to the strong anion-cation and weak π-cation interactions and high binding affinities. Nonpolar interactions (vdW and SA) are dominant in binding free energies. Complex solvation energy also has a crucial role in binding energies and might be attributed to the change in the structure of the complexes.

We also analyzed hydrogen interactions to observe their effect on the structure of the oligomers when they went to complexation with ssDNAs. S–H interactions are predominant. There are almost no O–H interactions in all complexes. In other words, ssDNAs approach oligomers from their backbones upon complexation. In addition to these results, no remarkable change was observed when the imidazole derivative replaced the cationic amine moiety side group.

Declaration of competing interest

The authors declare the following financial interests/personal relationships which may be considered as potential competing interests: Nuran ElmaciIrmak reports financial support was provided by Scientific and Technological Research Council of Turkey

Table 3
Binding free energies and their decompositions of complexes (kcal/mol).

	O1_20A		O1_20T		O2_20A		O2_20T	
	Mean	SD	Mean	SD	Mean	SD	Mean	SD
Elec:	−5370.93	105.32	−5341.19	69.50	−5597.53	53.84	−5505.94	82.90
vdW:	−45.55	4.66	−47.68	5.06	−53.57	3.92	−37.10	5.28
PB:	5347.34	108.30	5317.00	71.36	5590.16	57.68	5480.47	84.65
SA:	−5.35	0.51	−5.67	0.53	−6.11	0.43	−4.91	0.60
Total:	−74.50	5.89	−77.55	5.30	−67.05	7.85	−67.48	7.07

Data availability

The authors do not have permission to share data.

Acknowledgments

This work was supported by the "Scientific and Technological Research Council of Turkey", TUBITAK, under project numbers 119Z100. The numerical calculations reported in this paper were entirely performed at TUBITAK ULAKBIM, High Performance and Grid Computing Center (TRUBA resources). Computing resources used in this work were provided by the National Center for High Performance Computing of Turkey (UHeM) under grant number #1014132022#. We want to thank to Ümit Hakan Yıldız for the inspiration for this study.

Appendix A. Supplementary data

Supplementary data to this article can be found online at https://doi.org/10.1016/j.jmgm.2023.108501.

References

[1] F. Feng, F. He, L. An, S. Wang, Y. Li, D. Zhu, Fluorescent conjugated polyelectrolytes for biomacromolecule detection, Adv. Mater. 20 (2008) 2959–2964, https://doi.org/10.1002/adma.200800624.
[2] J. Rubio-Magnieto, A. Thomas, S. Richeter, A. Mehdi, P. Dubois, R. Lazzaroni, S. Clément, M. Surin, Chirality in DNA–π-conjugated polymer supramolecular structures: insights into the self-assembly, Chem. Commun. 49 (2013) 5483, https://doi.org/10.1039/c3cc42108b.
[3] D. Rajwar, G. Ammanath, J.A. Cheema, A. Palaniappan, U.H. Yildiz, B. Liedberg, Tailoring conformation-induced chromism of polythiophene copolymers for nucleic acid assay at resource limited settings, ACS Appl. Mater. Interfaces 8 (2016) 8349–8357, https://doi.org/10.1021/acsami.5b12171.
[4] A.C. Carreon, W.L. Santos, J.B. Matson, R.C. So, Cationic polythiophenes as responsive DNA-binding polymers, Polym. Chem. 5 (2014) 314–317, https://doi.org/10.1039/C3PY01069D.
[5] S.W. Thomas, G.D. Joly, T.M. Swager, Chemical sensors based on amplifying fluorescent conjugated polymers, Chem. Rev. 107 (2007) 1339–1386, https://doi.org/10.1021/cr0501339.
[6] H.A. Ho, M. Béra-Abérem, M. Leclerc, Optical sensors based on hybrid DNA/conjugated polymer complexes, Chem. Eur J. 11 (2005) 1718–1724, https://doi.org/10.1002/chem.200400537.
[7] T. Ma, C. Li, G. Shi, Optically active supramolecular complex formed by ionic self-assembly of cationic perylenediimide derivative and adenosine triphosphate, Langmuir 24 (2008) 43–48, https://doi.org/10.1021/la702559m.
[8] X. Wang, Q. Feng, L. Wang, M. Pei, J. Zhao, G. Zhang, A novel polythiophene derivative as a sensitive colorimetric and fluorescent sensor for the detection of ATP, Des. Monomers Polym. 17 (2014) 26–32, https://doi.org/10.1080/15685551.2013.771315.
[9] O.R. Miranda, C.C. You, R. Phillips, I.B. Kim, P.S. Ghosh, U.H.F. Bunz, V.M. Rotello, Array-based sensing of proteins using conjugated polymers, J. Am. Chem. Soc. 129 (2007) 9856–9857, https://doi.org/10.1021/ja0737927.
[10] J. Rubio-Magnieto, E.G. Azene, J. Knoops, S. Knippenberg, C. Delcourt, A. Thomas, S. Richeter, A. Mehdi, P. Dubois, R. Lazzaroni, D. Beljonne, S. Clément, M. Surin, Self-assembly and hybridization mechanisms of DNA with cationic polythiophene, Soft Matter 11 (2015) 6460–6471, https://doi.org/10.1039/c5sm01484k.
[11] W. Zheng, L. He, Quantitative measurements of thermodynamics and kinetics of polythiophene–DNA complex formation in DNA detection, Biomater. Sci. 2 (2014) 1471, https://doi.org/10.1039/C4BM00210E.
[12] G. Ammanath, C.G. Delachi, S. Karabacak, Y. Ali, B.O. Boehm, U.H. Yildiz, P. Alagappan, B. Liedberg, Colorimetric and fluorometric profiling of advanced glycation end products, ACS Appl. Mater. Interfaces 14 (2022) 94–103, https://doi.org/10.1021/acsami.1c16261.
[13] J. Preat, D. Zanuy, E.A. Perpete, C. Aleman, Binding of cationic conjugated polymers to DNA: atomistic simulations of adducts involving the Dickerson's dodecamer, Biomacromolecules 12 (2011) 1298–1304, https://doi.org/10.1021/bm200022n.
[14] E. Kıbrıs, N.N. Barbak, N.E. Irmak, CHARMM force field generation for a cationic thiophene oligomer with ffTK, J. Mol. Model. 27 (2021), https://doi.org/10.1007/s00894-020-04610-2.
[15] K. Vanommeslaeghe, E. Hatcher, C. Acharya, S. Kundu, S. Zhong, J. Shim, E. Darian, O. Guvench, P. Lopes, I. Vorobyov, A.D. Mackerell, CHARMM general force field: a force field for drug-like molecules compatible with the CHARMM all-atom additive biological force fields, J. Comput. Chem. 8 (2009), https://doi.org/10.1002/jcc.21367. NA-NA.
[16] C.G. Mayne, J. Saam, K. Schulten, E. Tajkhorshid, J.C. Gumbart, Rapid parameterization of small molecules using the force field toolkit, J. Comput. Chem. 34 (2013) 2757–2770, https://doi.org/10.1002/jcc.23422.
[17] C.G. Mayne, M. Muller, E. Tajkhorshid, Parameterizing Small Molecules Using the Force Field Toolkit (ffTK), University of Illinois at Urbana-Champaign, 2015.
[18] A. Pavlova, J.C. Gumbart, Parametrization of macrolide antibiotics using the force field toolkit, J. Comput. Chem. 36 (2015) 2052–2063, https://doi.org/10.1002/jcc.24043.
[19] M.J. Frisch, G.W. Trucks, H.B. Schlegel, G.E. Scuseria, M.A. Robb, J.R. Cheeseman, G. Scalmani, V. Barone, B. Mennucci, G.A. Petersson, H. Nakatsuji, M. Caricato, X. Li, H.P. Hratchian, A.F. Izmaylov, J. Bloino, G. Zheng, J.L. Sonnenberg, M. Hada, M. Ehara, K. Toyota, R. Fukuda, J. Hasegawa, M. Ishida, T. Nakajima, Y. Honda, O. Kitao, H. Nakai, T. Vreven, J.A. Montgomery Jr., J.E. Peralta, F. Ogliaro, M. Bearpark, J.J. Heyd, E. Brothers, K.N. Kudin, V.N. Staroverov, T. Keith, R. Kobayashi, J. Normand, K. Raghavachari, A. Rendell, J.C. Burant, S.S. Iyengar, J. Tomasi, M. Cossi, N. Rega, J.M. Millam, M. Klene, J.E. Knox, J.B. Cross, V. Bakken, C. Adamo, J. Jaramillo, R. Gomperts, R.E. Stratmann, O. Yazyev, A. J. Austin, R. Cammi, C. Pomelli, J.W. Ochterski, R.L. Martin, K. Morokuma, V. G. Zakrzewski, G.A. Voth, P. Salvador, J.J. Dannenberg, S. Dapprich, A.D. Daniels, O. Farkas, J.B. Foresman, J.v. Ortiz, J. Cioslowski, J.D. Fox, Gaussian 09, Revision A, 2009. Wallingford CT, Gaussian 09, Revision A, Wallingford CT.
[20] W.L. Jorgensen, J. Chandrasekhar, J.D. Madura, R.W. Impey, M.L. Klein, Comparison of simple potential functions for simulating liquid water, J. Chem. Phys. 79 (1983) 926–935, https://doi.org/10.1063/1.445869.
[21] R.B. Best, X. Zhu, J. Shim, P.E.M. Lopes, J. Mittal, M. Feig, A.D. MacKerell, Optimization of the additive CHARMM all-atom protein force field targeting improved sampling of the backbone φ, ψ and side-chain χ1and χ2Dihedral Angles, J. Chem. Theor. Comput. 8 (2012) 3257–3273, https://doi.org/10.1021/ct300400x.
[22] M.D. Hanwell, D.E. Curtis, D.C. Lonie, T. Vandermeersch, E. Zurek, G.R. Hutchison, Avogadro : an Advanced Semantic Chemical Editor , Visualization , and Analysis Platform, 2012, pp. 1–17.
[23] J.C. Phillips, R. Braun, W.E.I. Wang, J. Gumbart, E. Tajkhorshid, E. Villa, C. Chipot, R.D. Skeel, H. Poincare, Scalable Molecular Dynamics with NAMD, 2005, https://doi.org/10.1002/jcc.20289.
[24] W. Humphrey, A. Dalke, K. Schulten, VMD: Visual Molecular Dynamics, 1996.
[25] J. Srinivasan, T.E. Cheatham, P. Cieplak, P.A. Kollman, D.A. Case, Continuum solvent studies of the stability of DNA, RNA, and phosphoramidate-DNA helices. https://pubs.acs.org/sharingguidelines, 1998.
[26] H. Liu, T. Hou, CaFE: a tool for binding affinity prediction using end-point free energy methods, Bioinformatics 32 (2016) 2216–2218, https://doi.org/10.1093/bioinformatics/btw215.